Journal of Power Sources 240 (2013) 204–211

Contents lists available at SciVerse ScienceDirect

Journal of Power Sources

journal homepage: www.elsevier.com/locate/jpowsour

Heat treatment of electrospun Polyvinylidene fluoride fibrous membrane separators for rechargeable lithium-ion batteries

Yinzheng Liang [a], Sichen Cheng [a], Jianmeng Zhao [a], Changhuan Zhang [a], Shiyuan Sun [a], Nanting Zhou [a], Yiping Qiu [a,*], Xiangwu Zhang [b,*]

[a] Department of Textile Materials Science and Product Design, College of Textile, Donghua University, Shanghai 201620, China
[b] Fiber and Polymer Science Program, Department of Textile Engineering, Chemistry and Science, North Carolina State University, Raleigh, NC 27695-8301, USA

HIGHLIGHTS

- Heat treatment was introduced to improve the mechanical properties of electrospun PVDF fibrous membrane separators.
- Heat-treated PVDF fibrous membranes exhibit high electrochemical oxidation limit.
- Heat-treated PVDF fibrous membranes have low interfacial resistance with lithium electrode.
- Li/$LiFePO_4$ cells using heat-treated PVDF fibrous membranes show high charge/discharge capacities and good cycle performance.

ARTICLE INFO

Article history:
Received 30 January 2013
Received in revised form
25 February 2013
Accepted 5 April 2013
Available online 12 April 2013

Keywords:
Lithium-ion battery
Electrospinning
PVDF
Separator
Heat treatment

ABSTRACT

Polyvinylidene fluoride (PVDF) fibrous membranes for use as lithium-ion battery separators were prepared by electrospinning technique. Heat treatment was introduced to improve the tensile strength and elongation-at-break as well as the tensile modulus of PVDF fibrous membranes, with the best mechanical properties achieved after treatment at 160 °C for 2 h. After heat treatment at 160 °C for 2 h, the ionic conductivity of the liquid electrolyte-soaked PVDF fibrous membranes was 1.35×10^{-3} S cm^{-1} at room temperature. Moreover, compared with commercial Celgard 2400 separator, heat-treated PVDF fibrous membranes exhibited higher electrochemical stability window and lower interfacial resistance with lithium electrode. In addition, at a 0.2C rate, Li/$LiFePO_4$ cells using heat-treated PVDF fibrous membrane separator showed high charge/discharge capacities and stable cycle performance.

1. Introduction

Separator is a critical component in rechargeable lithium-ion batteries and it plays an important role in determining the battery performance [1–3]. The main function of a separator is to keep the positive and negative electrodes apart to prevent electrical short circuits while enabling free ionic transport [1–3]. Currently, most commercial separators are based on microporous membranes made from polyolefins such as polyethylene and polypropylene [4–6]. These polyolefin separators have good mechanical strength, suitable thickness, and excellent chemical stability [7–9]. However, they have several disadvantages including low porosity, unsatisfactory thermal stability, and poor wettability in liquid electrolytes [7–9]. These disadvantages cause high cell resistance and restrict the performance of lithium-ion batteries. As a result, to obtain high-performance lithium-ion batteries, alternative separators with excellent overall properties are needed.

In recent years, electrospinning has been widely used as a new method to prepare fibrous membranes for use as separators in lithium-ion batteries [10,11]. Electrospun fibrous membranes have high porosities, large specific surface areas and interconnected porous structures, and as a result, they are able to uptake large amounts of liquid electrolytes and offer effective conduction channels, which in turn lead to high ionic conductivities and good electrochemical properties [10,11]. Many polymers such as polyacrylonitrile (PAN), polyethylene oxide (PEO), polymethyl methacrylate (PMMA), polyvinylidene fluoride (PVDF) and polyvinyl alcohol (PVA), etc., have been used as the host polymer for the preparation of electrospun fibrous membranes as separators for

* Corresponding authors.
E-mail addresses: ypqiu@dhu.edu.cn (Y. Qiu), xiangwu_zhang@ncsu.edu (X. Zhang).

0378-7753/$ – see front matter © 2013 Elsevier B.V. All rights reserved.
http://dx.doi.org/10.1016/j.jpowsour.2013.04.019

lithium-ion batteries [12–16]. Among these polymers, PVDF has attractive significant attention because of its good thermal and electrochemical stabilities, and excellent affinity to electrolyte solutions [17,18]. Moreover, PVDF-based separators contain fluorine atoms and have excellent anodic stability and high dielectric constant ($\varepsilon = 8.6$), assisting the ionization of lithium salts [19–21]. However, the practical use of electrospun PVDF fibrous membranes is restricted by their insufficient mechanical properties. Electrospun PVDF fibrous membranes are inherently weak and cannot withstand the large tension developed by the winding operation during battery assembly [22].

In this study, heat treatment was used to improve the mechanical properties of electrospun PVDF fibrous membranes. It was found that heat treatment of PVDF fibrous membranes significantly improved their tensile strength and elongation-at-break as well as the tensile modulus. The influence of heat treatment on the morphology and electrochemical performance of PVDF fibrous membranes was also investigated. Results demonstrated that heat-treated PVDF fibrous membranes are promising separator candidate with improved mechanical properties and excellent electrochemical performance.

2. Experimental

2.1. Membrane preparation and heat treatment

Polyvinylidene fluoride (PVDF, MW = 400,000, Kynar 761) was purchased from Sinopharm Chemical Reagent Co., Ltd., and was vacuum dried at 60 °C for 12 h before use. N,N-Dimethylacetamide (DMAc) and acetone were purchased from Sinopharm Chemical Reagent Co., Ltd., and they were used as received without further purification.

PVDF was dissolved in a mixed solvent of DMAc/acetone (7:3, V/V) to obtain a 12 wt.% solution, which was stirred for 12 h at 60 °C. During electrospinning, the solution was fed in a 10 ml syringe and delivered with a flow rate of 0.4 ml h^{-1} under applied voltage of 16 kV. The distance between the needle tip and the collector was 20 cm. The electrospun fibers were accumulated on the collector, forming free-standing fibrous membranes. The resultant PVDF fibrous membranes were then dried under vacuum at 60 °C for 12 h to remove the solvent residual before further use.

The heat treatment of PVDF fibrous membranes was carried out under vacuum, and the heat treatment conditions were shown in Table 1.

2.2. Structure characterization

The morphology of PVDF fibrous membranes before and after heat treatment was observed by scanning electron microscope (SEM, TM-1000, and Hitachi) with an accelerating voltage of 5 kV. The crystal structure variation of the PVDF fibrous membranes before and after heat treatment was identified by differential scanning calorimeter (DSC, PE7, Perkin–Elmer Co., U.S.A) with a heating rate of 10 °C min^{-1} over a temperature range of 50–200 °C under nitrogen atmosphere. The crystallinity was calculated based on:

$$\chi_c = \frac{\Delta H_f}{\Delta H_f^*} \times 100\% \quad (1)$$

where ΔH_f is the measured melting enthalpy of PVDF fibrous membrane, and ΔH_f^* the melting enthalpy (104.7 J g^{-1}) of 100% crystalline PVDF. The wide-angle X-ray diffraction (WXRD, RIGAKU, Japan) was carried on a D/Max-2550 PC X-ray diffractometer recorded using CuKα radiation with an experimental condition of 45 kV and 50 mA, at a scanning rate of 2° min^{-1} and 2θ range of 5–90°.

The porosities of PVDF fibrous membranes were determined by soaking them in *n*-butanol for 2 h until equilibrium was achieved at room temperature. The excess *n*-butanol adhering to the membrane surface was gently removed with wipes. The porosity (*P*%) was calculated by:

$$P\% = \frac{W_w - W_d}{\rho_b \times V_m} \times 100\% \quad (2)$$

where W_w and W_d were the weights of the electrolyte-soaked membrane and dry membrane, respectively, ρ_b the density of *n*-butanol, and V_m the volume of the dry membrane.

2.3. Mechanical property tests

Tensile strengths, moduli and elongations-at-break of PVDF fibrous membranes were determined by an electronic tensile strength tester (XQ-2 Fiber Tensile Testing Machine, Shanghai, China). Measurements were carried out with a crosshead speed of 5 mm min^{-1} and gauge length of 30 mm. The reported values were the averages of at least five specimens for each sample.

2.4. Electrolyte uptake measurements

The liquid electrolyte uptakes of PVDF fibrous membranes were measured by soaking them in a liquid electrolyte of 1 mol L^{-1} $LiPF_6$–ethylene carbonate (EC)/dimethyl carbonate (DMC) (1:1 by volume) for 4 h. The liquid electrolyte uptake was calculated based on:

$$EU = \frac{W_1 - W_0}{W_0} \times 100\% \quad (3)$$

where W_1 and W_0 were the weights of the electrolyte-soaked membrane and dry membrane, respectively.

2.5. Electrochemical performance evaluation

The ionic conductivities of liquid electrolyte-soaked PVDF fibrous membranes were measured by electrochemical impedance spectroscopy using a CHI 660D electrochemical workstation (Shanghai Chenhua Instrument Inc., China). The membranes were placed between two stainless steel blocking electrodes, and spectra were obtained by sweeping from 100 kHz to 0.1 Hz with an AC amplitude of 10 mV at room temperature. The ionic conductivity (σ) was calculated from the following equation:

$$\sigma = \frac{d}{R_b \times S} \quad (4)$$

where R_b is the bulk resistance, and *d* and *S* are the thickness and area of the fibrous membrane, respectively.

Table 1
Temperatures and times used for the heat treatment of PVDF fibrous membranes.

Sample no.	Heat treatment temperature (°C)	Heat treatment time (h)
A (Untreated)	–	–
B (Heat-treated at 150 °C)	150	2
C (Heat-treated at 155 °C)	155	2
D (Heat-treated at 160 °C)	160	2

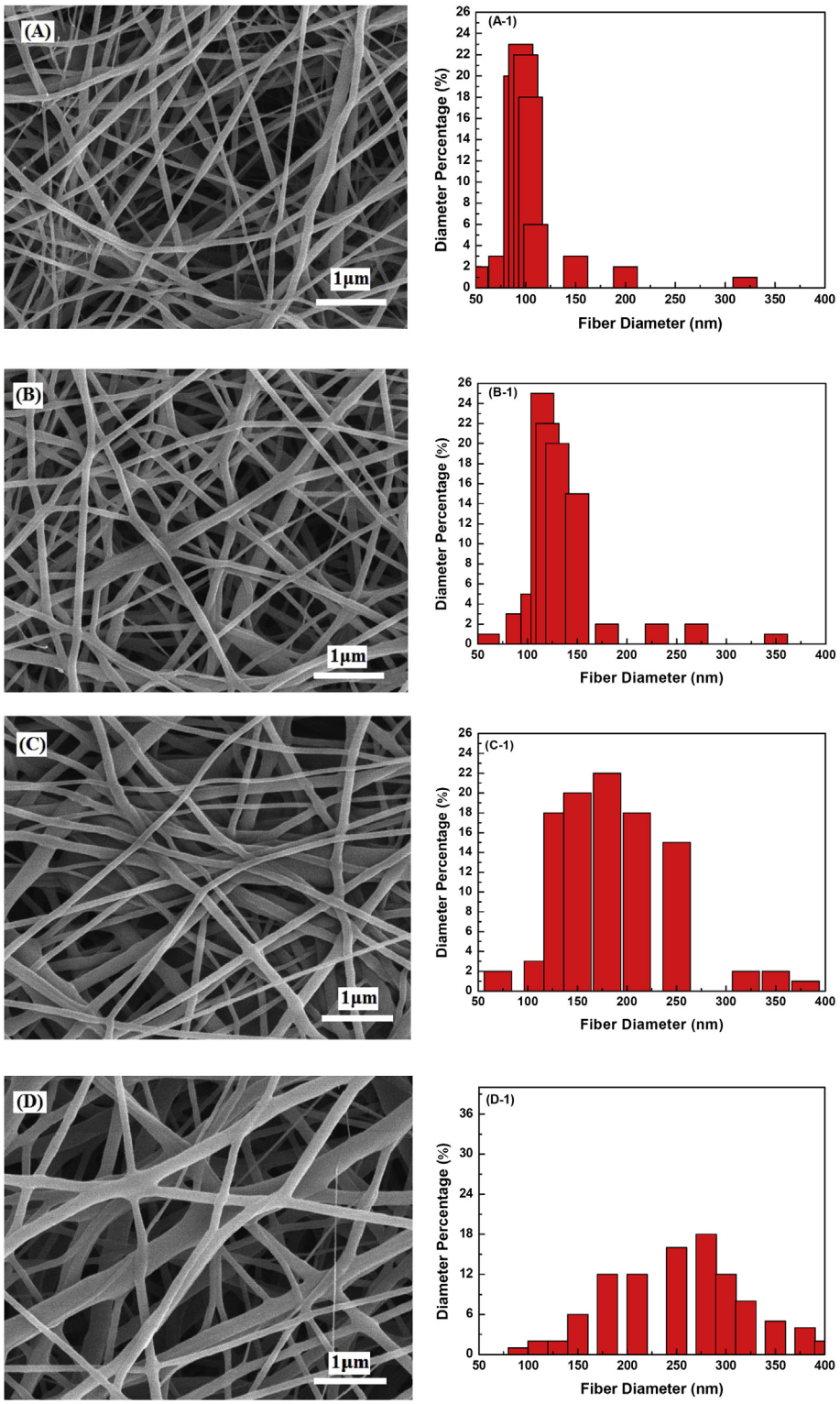

Fig. 1. SEM images and fiber diameter distributions of PVDF fibrous membranes: (A, A-1) untreated, (B, B-1) heat-treated at 150 °C, (C, C-1) heat-treated at 155 °C, and (D, D-1) heat-treated at 160 °C.

Electrochemical stability was determined using linear sweep voltammetry. The measurements were carried out by using stainless steel as the blocking working electrode, and lithium metal as both the counter and the reference electrode. An electrochemical analyzer CHI 660D (Shanghai Chenhua Instrument Inc. China) was used to record the electrochemical stability under the scan rate of 1 mV s^{-1} and over the potential range of 2.5–6.0 V versus Li^+/Li at room temperature.

The interfacial resistances between liquid electrolyte-soaked PVDF fibrous membranes and lithium metal electrode were measured by monitoring the impedance of symmetrical lithium cells under open-circuit conditions. The measurements were

carried out over a frequency range of 65 kHz to 0.1 Hz using an electrochemical analyzer CHI 660D (Shanghai Chenhua Instrument Inc. China). Prior to the measurements, all symmetric lithium cells rested at room temperature for 24 h.

The electrochemical performance of lithium/lithium iron phosphate ($LiFePO_4$) cells containing liquid electrolyte-soaked PVDF fibrous membranes was evaluated using CR2032 coin cells (Hohsen Corp). Coin cells were assembled by sandwiching liquid electrolyte-soaked PVDF fibrous membranes between lithium metal anode and $LiFePO_4$ cathode. The $LiFePO_4$ electrode consisted of active material $LiFePO_4$ (80 wt.%, Hydro-Québec), acetylene black (10 wt.%, Fisher Scientific) and polyvinylidene fluoride binder (10 wt.%, Aldrich). The charge/discharge performance of coin cells was examined using the LAND battery cycle system (Wuhan Blue Electric co., LTD, China) at potentials ranging from 2.5 to 4.2 V at 0.2C rate.

3. Results and discussion

3.1. Morphology

Fig. 1 presents SEM images of PVDF fibrous membranes before and after heat treatment at three different temperatures (150, 155, and 160 °C), which are around the melting temperature of PVDF powder (159.5 °C). With increase in heat treatment temperature, the average fiber diameter increases and the fiber diameter distribution becomes wider. This phenomenon is due to the fiber shrinkage occurred at elevated temperatures. From the SEM images, it is also seen that more interconnected fiber adherence is formed in heat-treated PVDF fibrous membranes.

3.2. Crystal structure

Fig. 2 shows the DSC curves of PVDF powder and PVDF fibrous membranes before and after heat treatment. The melting temperature, melting enthalpy and crystallinity obtained from the DCS curves are shown in Table 2. It is seen that melting temperature, melting enthalpy and crystallinity of PVDF fibrous membranes are higher than those of PVDF powder. This is probably because the molecular chains were largely stretched by the high electrostatic field during the spinning process, which could lead to orientation-induced crystallization.

Table 2
Thermal properties and degrees of crystallinity of PVDF fibrous membranes.

Sample no.	Melting temperature (°C)	Melting enthalpy ($J\ g^{-1}$)	Crystallinity (%)	
			DSC	WAXD
PVDF powder	159.5	23.4	22.3	–
A (Untreated)	161.4	35.7	34.1	42.1
B (Heat-treated at 150 °C)	161.7	45.4	43.3	53.5
C (Heat-treated at 155 °C)	162.7	53.0	50.6	58.1
D (Heat-treated at 160 °C)	166.3	36.1	34.6	33.00

As shown in Fig. 2 and Table 2, the melting temperature of PVDF fibrous membranes increases with increase in heat treatment temperature. In addition, a shoulder melting peak emerges when the heat temperature is 150 or 155 °C, which is probably caused by the formation of unstable secondary crystals during the heat treatment process. The emergence of shoulder melting peak results in increased melting enthalpy and crystallinity for membranes heat-treated 150 and 155 °C. However, when the heat treatment temperature is 160 °C, the shoulder melting peak disappears, and as a result, the melting enthalpy and crystallinity decrease.

To further investigate the crystal structure variation of PVDF fibrous membranes, wide-angle X-ray diffraction (WAXD) data were obtain and are shown in Fig. 3. It has been reported that five crystal phases α, β, γ, δ and ε exist for PVDF and they can inter-transform under certain conditions [23,24]. It is seen from Fig. 3 that all four WAXD patterns exhibit a sharp peak at around 20.7°, which is a characteristics peak of PVDF β-phase crystalline structure, corresponding to the β(200/110). Other main X-ray diffraction peaks observed include 2θ = 18.6°, 26.7°, 36.6°, and 56.1°, which are ascribed to α(020), α(021), α(200), and β(221), respectively. This result indicates that α-phase and β-phase crystals co-exist in PVDF fibrous membranes. From Fig. 3, it is also seen that with increase in heat treatment temperature, the diffraction intensities of α peaks decrease while those of β peaks increase first and then decrease, with the maximum intensities achieved when the heat treatment temperature is 155 °C.

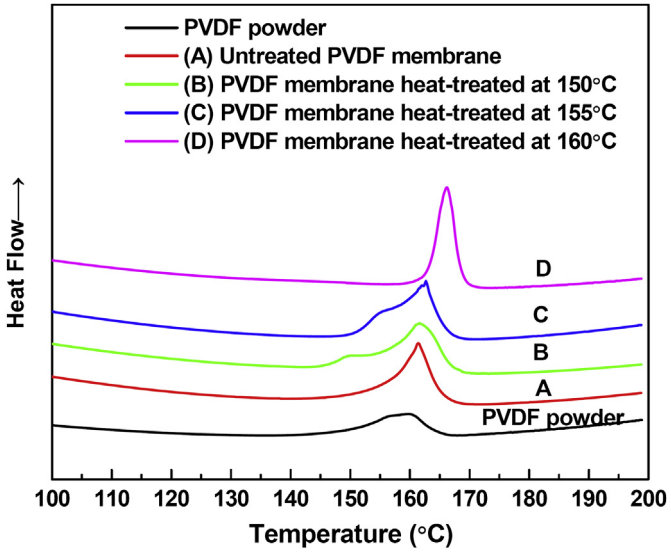

Fig. 2. DSC thermograms of PVDF power and PVDF fibrous membranes before and after heat treatment at different temperatures.

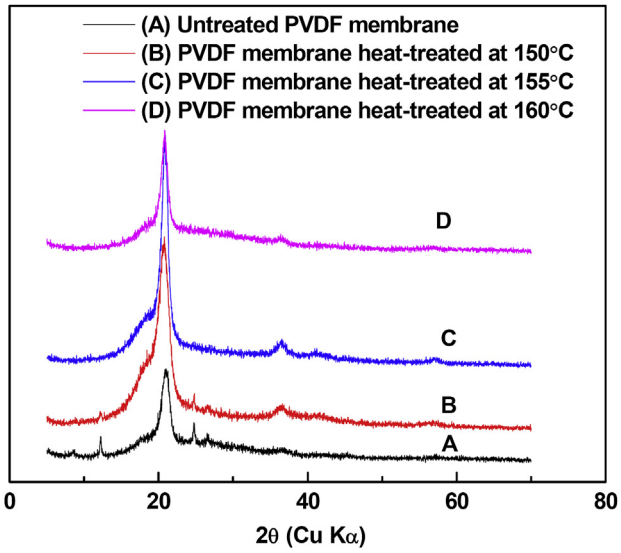

Fig. 3. WAXD patterns of PVDF fibrous membranes before and after heat treatment at different temperatures.

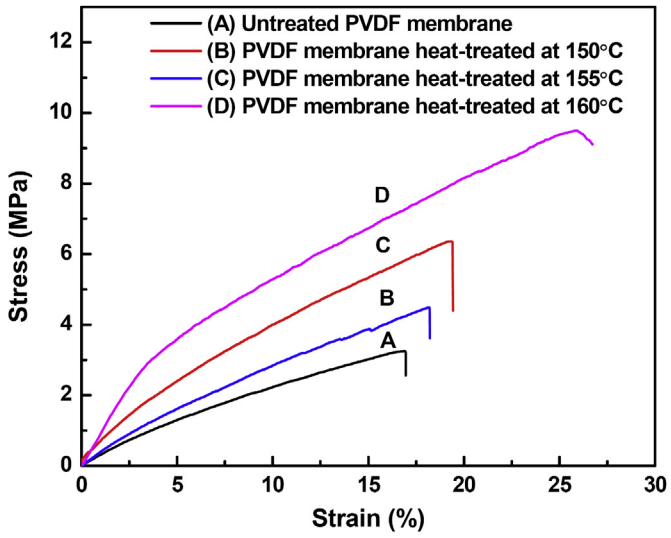

Fig. 4. Stress–strain curves of PVDF fibrous membranes before and after heat treatment at different temperatures.

3.3. Tensile properties

The tensile properties of PVDF fibrous membranes were measured. Fig. 4 shows the stress–strain curves of PVDF fibrous membranes before and after heat treatment. The tensile strength, modulus and elongation-at-break values are shown in Table 3. It is seen that heat treatment increases the tensile strength and tensile modulus as well as the elongation-at-break. In addition, the tensile strength, the tensile modulus and elongation-at-break of the PVDF fibrous membranes increase with increase in heat treatment temperature. The improvement in tensile properties for heat-treated PVDF fibrous membranes is the result of the increased fiber diameter, the formation of interfiber bonding, and the enhanced crystallinity. Firstly, the increase in fiber diameter can help the membranes bear more load, leading to increased membrane tensile strength. Secondly, the enhanced interfiber bonding makes the movement of the fibers more difficult, thereby making the fibrous membranes more rigid [26]. Thirdly, the higher crystallinity after heat treatment also contributes to the increased tensile strength and modulus [25].

3.4. Porosity and electrolyte uptake

The results of porosity measurements are presented in Table 4. It is seen that the porosity of the PVDF fibrous membranes decreases slightly with increase in heat treatment temperature. The decrease in membrane porosity is mainly caused by the increased fiber diameter after heat treatment. Although the porosity decreases after heat treatment, the lowest porosity (80.3%) achieved at a heat treatment temperature of 160 °C is still significantly higher than those of commercial separators (e.g., Celgard 2400: 40%).

Table 3
Tensile properties of PVDF fibrous membranes.

Sample no.	Tensile strength (MPa)	Young's modulus (MPa)	Elongation (%)
A (Untreated)	3.25	38.9	16.9
B (Heat-treated at 150 °C)	4.49	48.1	18.2
C (Heat-treated at 155 °C)	6.36	84.7	19.4
D (Heat-treated at 160 °C)	9.50	94.2	26.7

Table 4
Porosities of PVDF fibrous membranes.

Sample no.	Porosity (°C)
A (Untreated)	84.1
B (Heat-treated at 150 °C)	83.5
C (Heat-treated at 155 °C)	82.9
D (Heat-treated at 160 °C)	80.3

Fig. 5 shows the liquid electrolyte uptakes of PVDF fibrous membranes before and after heat treatment. In the PVDF fibrous membranes, the majority of liquid electrolyte is distributed in the open pores. However, the PVDF fibers may also absorb a small amount of liquid electrolyte to form a gel-like structure. From Fig. 5, it is seen that the liquid electrolyte uptake of PVDF fibrous membranes decreases slightly with increase in heat treatment temperature. This is mainly caused by the decreased membrane porosity since the amount of PVDF fibers does not change with heat treatment temperature.

3.5. Ionic conductivity

Fig. 6 shows the Nyquist curves of the liquid electrolyte-soaked PVDF fibrous membranes. The conductivity can obtained from the high-frequency intercept of the Nyquist curve on the z' axis. The untreated PVDF fibrous membrane has the highest ionic conductivity of 1.83×10^{-3} S cm^{-1} after being soaked in liquid electrolyte. With increase in heat treatment temperature, the ionic conductivity decreases slightly due to the decreased liquid electrolyte uptake. When heat treated at 160 °C, the ionic conductivity of liquid electrolyte-soaked PVDF fibrous membranes is the lowest (1.35×10^{-3} S cm^{-1}); however, it still higher than that (1.28×10^{-3} S cm^{-1}) of liquid electrolyte-soaked Celgard 2400. Therefore, the ionic conductivities of liquid electrolyte-soaked PVDF membranes can meet the conductivity requirement of lithium-ion battery applications. The relatively high ionic conductivities of liquid electrolyte-soaked electrospun fibrous membranes can be attributed to their high electrolyte uptake and fully interconnected pore structure.

3.6. Electrochemical stability

Fig. 7 shows the electrochemical stability windows of liquid electrolyte-soaked PVDF fibrous membranes before and after heat treatment at 160 °C. For comparison, the electrochemical stability

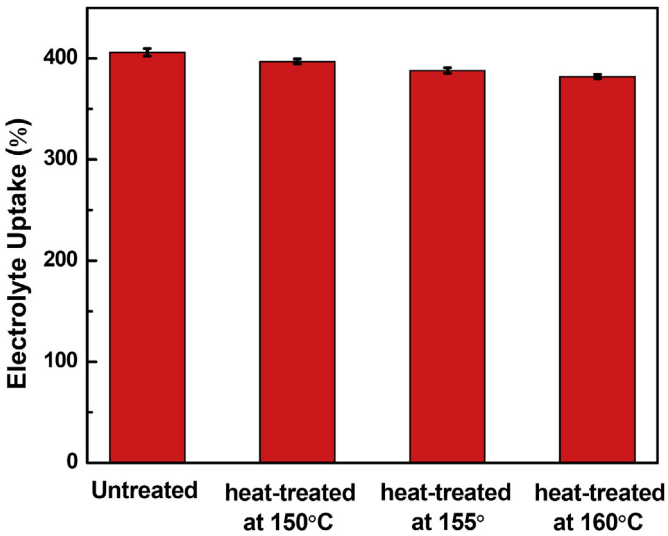

Fig. 5. Electrolyte uptakes of PVDF fibrous membranes before and after heat treatment at different temperatures.

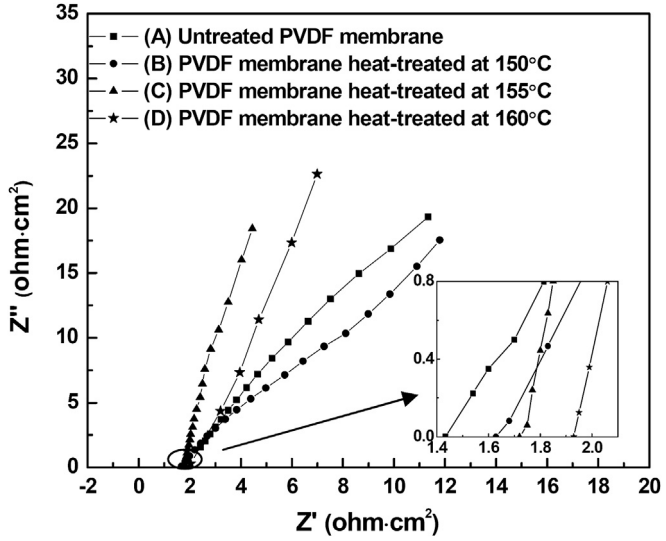

Fig. 6. Ionic conductivities of liquid electrolyte-soaked PVDF fibrous membranes.

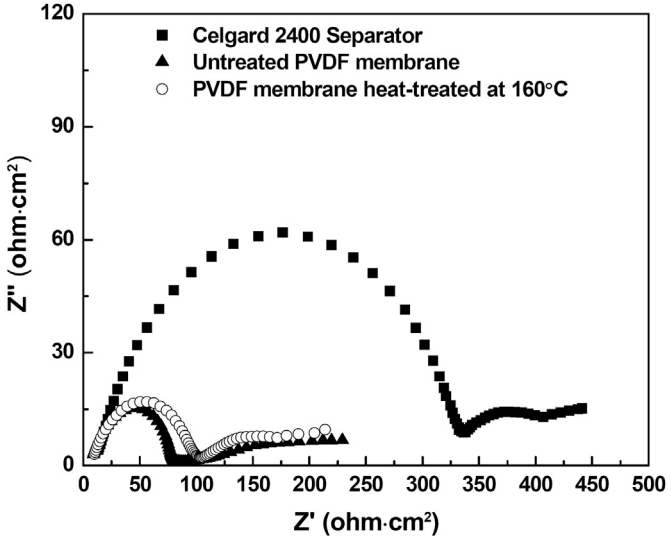

Fig. 8. Electrochemical impedance spectra of liquid electrolyte-soaked (a) Celgard 2400 separator, (b) untreated PVDF fibrous membrane, and (c) heat-treated (160 °C) PVDF fibrous membrane.

window of liquid electrolyte-soaked Celgard 2400 separator is also shown. The voltage corresponding to the onset of a steady increase in the observed current density indicates the electrochemical stability limit of the electrolyte-soaked membranes [11,27,28]. From Fig. 7, it can be found that both untreated and heat-treated PVDF fibrous membranes exhibit anodic stability up to 4.8 V versus Li^+/Li, which is greater than that (4.5 V) of Celgard 2400 separator. The high electrochemical stability of liquid electrolyte-soaked PVDF fibrous membranes should render them potentially compatible with most high-voltage cathode materials used for rechargeable lithium-ion batteries.

3.7. Interfacial resistance

The compatibility of liquid electrolyte-soaked PVDF fibrous membranes with lithium metal was investigated by measuring electrochemical impedance spectra (EIS) of Li/liquid electrolyte-soaked membrane/Li cells and the results are shown in Fig. 8. In an EIS curve, the left intercept on the z' axis of the intermediate-frequency semicircle represents the bulk resistance (R_b) while the diameter of the semicircle indicates the electrode–electrolyte interfacial resistance (R_{in}). As shown in Fig. 8, the order of R_{in} values is: untreated PVDF fibrous membrane (75.5 Ω cm^2) < heat-treated PVDF fibrous membrane (93.5 Ω cm^2) < Celgard 2400 separator (323 Ω cm^2). Both the untreated and heat-treated PVDF fibrous membranes show lower interfacial resistances than the commercial Celgard 2400 separator, which is due to their large porosities and high electrolyte uptakes, as well as the good membrane-electrode affinity [10,11].

3.8. Battery performance

In order to evaluate the feasibility of adopting PVDF fibrous membranes in practical rechargeable lithium-ion batteries, Li/$LiFePO_4$ cells using these membranes as the separator were fabricated and evaluated. For comparison, cells using commercial

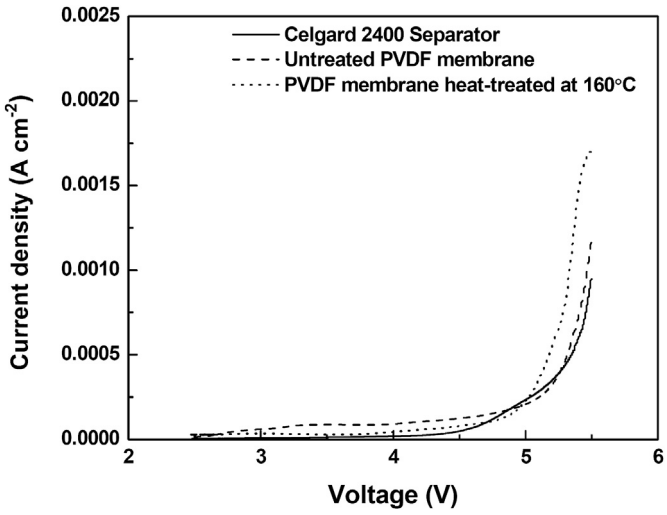

Fig. 7. Electrochemical stability windows of liquid electrolyte-soaked (a) Celgard 2400 separator, (b) untreated PVDF fibrous membrane, and (c) heat-treated (160 °C) PVDF fibrous membrane.

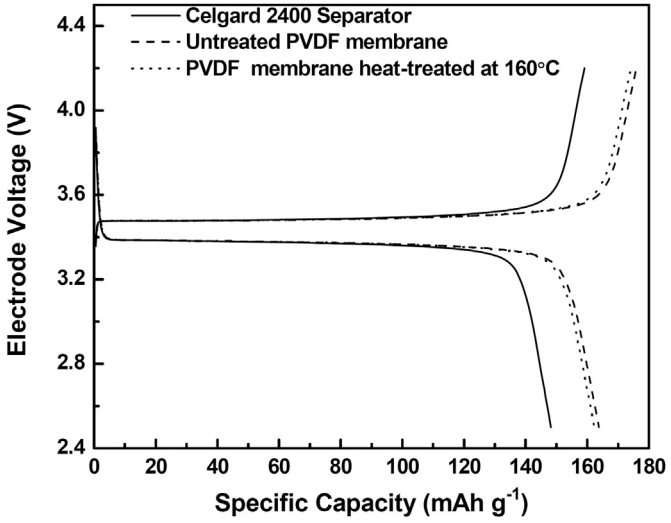

Fig. 9. First-cycle charge and discharge capacities of Li/$LiFePO_4$ cells with liquid electrolyte-soaked Celgard 2400 separator, untreated PVDF fibrous membrane, and heat-treated (160 °C) PVDF fibrous membrane.

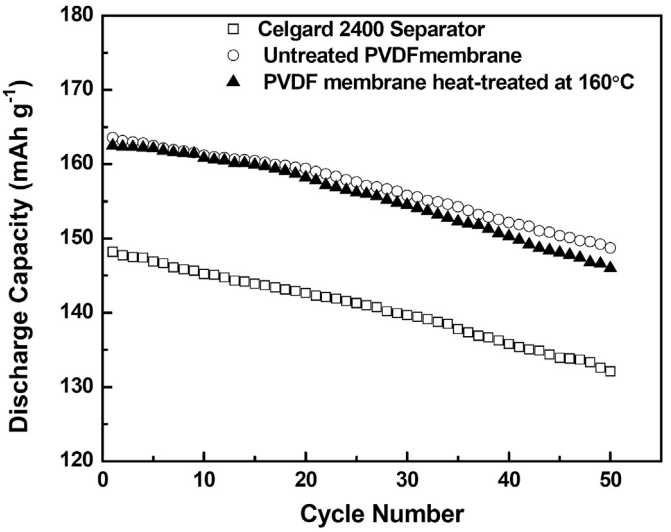

Fig. 10. Cycle performance of Li/$LiFePO_4$ cells containing liquid electrolyte-soaked Celgard 2400 separator, untreated PVDF fibrous membrane, and heat-treated (160 °C) PVDF fibrous membrane.

Celgard 2400 separator were also tested. The first-cycle charge/discharge capacity curves at a current density corresponding to 0.2C-rate are showed in Fig. 9. It is seen that the first-cycle charge and discharge capacities of cells containing heat-treated PVDF fibrous membranes are 168.2 and 162.3 mAh g^{-1}, respectively, which are higher than those (159.1 and 138.2 mAh g^{-1}) of cells containing Celgard 2400 separator and slightly lower than those (170.1 and 163.5 mAh g^{-1}) of cells containing untreated PVDF fibrous membranes. Heat-treated PVDF fibrous membranes have high porosities, large specific surface areas and interconnected porous structures, and as a result, they are able to uptake large amounts of liquid electrolytes and offer effective conduction channels, which in turn lead to high ionic conductivities and increased charge and discharge capacities. The effect of separator structure on the cathode capacitor has been observed by other researchers on different systems [11,29–33].

The discharge capacities as a function of cycle number are shown in Fig. 10 for Li/$LiFePO_4$ cells containing commercial Celgard separator and PVDF fibrous membranes. After 50 cycles, the cells using heat-treated PVDF fibrous membranes show a discharge capacity of 146 mAh g^{-1}, which is slightly lower than that (148.7 mAh g^{-1}) of cells using untreated PVDF fibrous membranes, but is significantly higher than that (133.2 mAh g^{-1}) of cells using commercial Celgard 2400 separator. The good cycle performance of PVDF fibrous membranes could be attributed to their unique porous structure, high liquid electrolyte uptake, and low interfacial resistance.

Table 5 compares the properties of heat-treated PVDF fibrous membrane and Celgard 2400. It is seen that the heat-treated PVDF fibrous membrane offers slight higher ionic conductivity than Celgard 2400, but it provides higher electrochemical stability window, lower resistance, and greater capacities.

Table 5
Comparison of heat-treated electrospun PVDF fibrous membrane with Celgard 2400. Heat treatment temperature: 160 °C.

	Celgard 2400	Heat-treated PVDF fibrous membrane
Ionic conductivity (25 °C) (S cm^{-1})	1.28×10^{-3}	1.35×10^{-3}
Electrochemical stability window (V)	4.5	4.8
Interfacial resistance (Ω cm^2)	93.5	75.5
First-cycle charge capacity (mAh g^{-1})	159.1	168.2
First-cycle discharge capacity (mAh g^{-1})	138.2	162.3
Fifth-cycle discharge capacity (mAh g^{-1})	133.2	146

4. Conclusion

The electrospinning technique was used to prepare PVDF fibrous membranes. In order to improve the mechanical properties, the resultant PVDF fibrous membranes were heat-treated at three different temperatures for 2 h. The tensile strength, tensile modulus and elongation-at-break of heat-treated PVDF fibrous membranes were higher than those of untreated fibrous membranes. After heat treatment at 160 °C for 2 h, the liquid electrolyte-soaked PVDF fibrous membranes showed a high ionic conductivity of 1.35×10^{-3} S cm^{-1} at room temperature, a good electrochemical stability up to 4.8 V versus Li^+/Li, and a relatively low interfacial resistance of 93.5 Ω cm^2. At a 0.2C rate, Li/$LiFePO_4$ cells using heat-treated PVDF fibrous membranes as the separator showed high first-cycle charge/discharge capacities and stable cycle performance. These results suggested that heat-treated PVDF fibrous membranes are promising separator candidate for high-performance lithium-ion batteries.

Acknowledgments

This work was supported by the National High Technology Research and Development Program of China (No. 2007AA03Z101), the State Key Program of National Natural Science of China (No. 51035003), Natural Science Foundation for the Youth (Nos. 50803010 and 60904056), National Science Foundation for Post-doctoral Scientists of China (No. 20100470664), Shanghai Post-doctoral Research Funded Project (No. 09R21410100), the Program of Introducing Talents of Discipline to Universities (No. B07024), Shanghai University Young Teacher Training Program, and the Fundamental Research Funds for the Central Universities.

References

[1] J.M. Tarascon, M. Armand, Nature 414 (2001) 359–367.
[2] S.S. Zhang, J. Power Sources 164 (2007) 351–363.
[3] P.K. Arora, Z.M. Zhang, Chem. Rev. 104 (2004) 4419–4462.
[4] A. Hasshimoto, K. Yagi, H. Mantoku, U.S. Patent, 6,048,607, 2000.
[5] S.Y. Lee, B.I. Ahn, S.G. Im, S.Y. Park, H.S. Song, Y.J. Kyung, U.S. Patent, 6,830,849, 2004.
[6] W.C. Yu, U.S. Patent, 6,878,226, 2005.
[7] F.G.B. Ooms, E.M. Kelder, J. Schoonman, N. Gerrits, J. Smedinga, G. Callis, J. Power Sources 598 (2001) 97–98.
[8] J. Saunier, F. Alloin, J.Y. Sanchez, G. Callis, J. Power Sources 451 (2003) 119–121.
[9] Y.M. Lee, J.W. Kim, N.S. Choi, J.A. Lee, W.H. Seol, J.K. Park, G. Callis, J. Power Sources 235 (2005) 139–140.
[10] P. Raghavan, X.H. Zhao, J. Manuel, C. Shin, M.Y. Heo, J.H. Ahn, Mater. Res. Bull. 45 (2010) 362–366.
[11] H.R. Jung, D.H. Ju, W.J. Lee, X.W. Zhang, R. Kotek, Electrochim. Acta 54 (2009) 3630–3637.
[12] Y.Z. Liang, L.W. Ji, B.K. Guo, Z. Lin, Y.F. Yao, Y. Li, Y.P. Yiu, X.W. Zhang, J. Power Sources 196 (2011) 436–441.
[13] A. Subramania, N.T.S. Kalyana, A.R.P. Sathiya, G.K. Vijaya, J. Membr. Sci. 294 (2007) 8–15.
[14] Y.Z. Liang, Z. Lin, Y.P. Yiu, X.W. Zhang, Electrochim. Acta 56 (2011) 6474–6480.
[15] P. Raghavan, J.W. Choi, J.H. Ahn, G. Cheruvally, G.S. Chauhan, H.J. Ahn, J. Power Sources 184 (2008) 437–443.
[16] Y.H. Ding, P. Zhang, Z.L. Long, Y. Jiang, F. Xu, W. Di, J. Membr. Sci. 329 (2009) 56–59.
[17] J.R. Kim, S.W. Choi, S.M. Jo, W.S. Lee, B.C. Kim, Electrochim. Acta 50 (2004) 69–75.
[18] C.R. Yang, Z.D. Jia, Z.C. Guan, L.M. Wang, J. Power Sources 189 (2009) 716–720.
[19] S. Ramesh, T. Winie, A.K. Arof, Eur. Polym. J. 43 (2007) 1963–1968.

[20] H.J. Rhoo, H.T. Kim, J.K. Park, T.S. Hwang, Electrochim. Acta 42 (1997) 1571–1579.
[21] S. Rajendran, R.S. Babu, P. Sivakumar, J. Membr. Sci. 315 (2008) 67–73.
[22] M. Alcoutlabi, H. Lee, J.V. Watson, X. Zhang, J. Mater. Sci. 48 (2013) 2690–2700.
[23] A.J. Lovinger, Macromolecules 15 (1982) 40–44.
[24] J. Hirschinger, D. Schaefer, H.W. Spiess, A.J. Lovinger, Macromolecules 24 (1991) 2428–2433.
[25] S.S. Choi, Y.S. Lee, C.W. Joo, S.G. Lee, J.K. Park, K.S. Han, Electrochim. Acta 50 (2004) 339–343.
[26] S.S. Choi, S.G. Lee, C.W. Joo, S.S. Im, S.H. Kim, J. Mater. Sci. 39 (2004) 1511–1516.
[27] X. Li, G. Cheruvally, J.K. Kim, J.W. Choi, J.H. Ahn, K.W. Kim, H.-J. Ahn, J. Power Sources 167 (2007) 491.
[28] G. Cheruvally, J.K. Kim, J.-W. Choi, J.H. Ahna, Y.J. Shin, J. Manuel, P. Raghavan, K.W. Kim, H.J. Ahn, D.S. Choi, C.E. Song, J. Power Sources 172 (2007) 863–869.
[29] P. Raghavan, X. Zhao, C. Shin, D.H. Baek, J.W. Choi, J. Manuel, M.Y. Heo, J.H. Ahn, C. Nah, J. Power Sources 195 (2010) 6088–6094.
[30] P. Raghavan, X. Zhao, J. Manuel, G.S. Chauhan, J.H. Ahn, H.S. Ryu, H.J. Ahn, K.W. Kim, C. Nah, Electrochim. Acta 55 (2010) 1347–1354.
[31] P. Raghavan, J. Manuel, X. Zhao, D.S. Kim, J.H. Ahn, C. Nah, J. Power Sources 196 (2011) 6742–6749.
[32] P. Carol, P. Ramakrishnan, B. John, G. Cheruvally, J. Power Sources 196 (2011) 10156–10162.
[33] D. Fu, B. Luan, S. Argue, M.N. Bureau, I.J. Davidson, J. Power Sources 206 (2012) 325–333.